

THE TRANSIT INGRESS AND THE TILTED ORBIT OF THE EXTRAORDINARILY ECCENTRIC EXOPLANET HD 80606b

JOSHUA N. WINN¹, ANDREW W. HOWARD^{2,3,15}, JOHN ASHER JOHNSON^{4,16}, GEOFFREY W. MARCY², J. ZACHARY GAZAK⁴,
DONN STARKEY⁵, ERIC B. FORD⁶, KNICOLE D. COLÓN⁶, FRANCISCO REYES⁶, LISA NORTMANN⁷, STEFAN DREIZLER⁷,
STEPHEN ODEWAHN⁸, WILLIAM F. WELSH⁹, SHIMONEE KADAKIA⁹, ROBERT J. VANDERBEL¹⁰, ELISABETH R. ADAMS¹¹,
MATTHEW LOCKHART¹¹, IAN J. CROSSFIELD¹², JEFF A. VALENTI¹³, RONALD DANTOWITZ¹⁴, AND JOSHUA A. CARTER¹

¹ Department of Physics, and Kavli Institute for Astrophysics and Space Research, Massachusetts Institute of Technology, Cambridge, MA 02139, USA

² Department of Astronomy, University of California, Mail Code 3411, Berkeley, CA 94720, USA

³ Space Sciences Laboratory, University of California, Berkeley, CA 94720, USA

⁴ Institute for Astronomy, University of Hawaii, Honolulu, HI 96822, USA

⁵ DeKalb Observatory H63, Auburn, IN 46706, USA

⁶ Department of Astronomy, University of Florida, 211 Bryant Space Center, P.O. Box 112055, Gainesville, FL 32611, USA

⁷ Institute for Astrophysics, Friedrich-Hund-Platz 1, D-37077 Göttingen, Germany

⁸ McDonald Observatory, University of Texas, Austin, TX 78712, USA

⁹ Department of Astronomy, San Diego State University, 5500 Campanile Drive, San Diego, CA 92182, USA

¹⁰ Department of Operations Research and Financial Engineering, Princeton University, Princeton, NJ 08544, USA

¹¹ Department of Earth, Atmospheric, and Planetary Science, Massachusetts Institute of Technology, Cambridge, MA 02139, USA

¹² Department of Astronomy, University of California, 430 Portola Plaza, Box 951547, Los Angeles, CA 90095, USA

¹³ Space Telescope Science Institute, 3700 San Martin Dr., Baltimore, MD 21218, USA

¹⁴ Clay Center Observatory, Dexter and Southfield Schools, 20 Newton St., Brookline, MA 02445, USA

Received 2009 July 14; accepted 2009 August 19; published 2009 September 16

ABSTRACT

We present the results of a transcontinental campaign to observe the 2009 June 5 transit of the exoplanet HD 80606b. We report the first detection of the transit ingress, revealing the transit duration to be 11.64 ± 0.25 hr and allowing more robust determinations of the system parameters. Keck spectra obtained at midtransit exhibit an anomalous blueshift, giving definitive evidence that the stellar spin axis and planetary orbital axis are misaligned. The Keck data show that the projected spin–orbit angle λ is between 32° and 87° with 68.3% confidence and between 14° and 142° with 99.73% confidence. Thus, the orbit of this planet is not only highly eccentric ($e = 0.93$) but is also tilted away from the equatorial plane of its parent star. A large tilt had been predicted, based on the idea that the planet’s eccentric orbit was caused by the Kozai mechanism. Independently of the theory, it is worth noting that all three exoplanetary systems with known spin–orbit misalignments have massive planets on eccentric orbits, suggesting that those systems migrate through a different channel than lower mass planets on circular orbits.

Key words: planetary systems – planetary systems: formation – stars: individual (HD 80606) – stars: rotation

Online-only material: color figures

1. INTRODUCTION

Discovered by Naef et al. (2001), HD 80606b is a giant planet of approximately 4 Jupiter masses whose orbit carries it within 7 stellar radii of its parent star. Yet it is no ordinary “hot Jupiter”: the other end of the planet’s 111-day orbit is about 30 times further away from the star. With an orbital eccentricity of 0.93, HD 80606b presents an extreme example of the “eccentric exoplanet” problem: the observation that exoplanets often have eccentric orbits, despite the 20th century expectation that more circular orbits would be common (Lissauer 1995).

Wu & Murray (2003) proposed that HD 80606b formed on a wide circular orbit that was subsequently shrunk and elongated by a combination of the Kozai (1962) effect and tidal friction. In this scenario, the gravitational perturbation from the companion star HD 80607 excites large-amplitude oscillations of the planet’s orbital eccentricity and inclination. During high-eccentricity phases, tidal friction drains the orbital energy and shrinks the orbit until the oscillations cease due to competing perturbations arising from stellar asphericity or general relativity. Fabrycky & Tremaine (2007) noted that a

probable consequence of this scenario is that the star–planet orbit was left tilted with respect to its original orbital plane, which was presumably aligned with the stellar equator. Hence, a demonstration that the planetary orbital axis and stellar spin axis are misaligned would be supporting evidence for the Kozai scenario.

For a transiting planet, it is possible to measure the angle between the sky projection of those two axes through observations of the Rossiter–McLaughlin (RM) effect, a distortion of spectral lines resulting from the partial eclipse of the rotating stellar surface (Rossiter 1924; McLaughlin 1924; Queloz et al. 2000; see Fabrycky & Winn 2009 for a recent summary of results). In a series of fortunate events, it recently became known that the orbit of HD 80606b is viewed close enough to edge-on to exhibit transits and thereby permit RM observations. First, Laughlin et al. (2009) detected an occultation of the planet by the star, an event that is visible from only 15% of the sight lines to HD 80606. Then three groups detected a transit (Moutou et al. 2009; Fossey et al. 2009; Garcia-Melendo & McCullough 2009), which was predicted to occur with only 15% probability even after taking into account the occurrence of occultations.

All three groups detected the transit egress, but not the ingress. The lack of information about the ingress, and hence the transit duration, hampered previous determinations of this system’s

¹⁵ Townes Postdoctoral Fellow.

¹⁶ NSF Astronomy and Astrophysics Postdoctoral Fellow.

parameters. In particular, Moutou et al. (2009) gathered radial-velocity (RV) data bracketing the transit egress that displays the RM effect, but due to the unknown transit duration it was not immediately clear whether meaningful constraints could be placed on the angle λ between the sky projections of the stellar spin axis and the orbital axis. Pont et al. (2009) concluded that λ is nonzero based on a Bayesian analysis of the available data, but their results were sensitive to prior assumptions regarding the stellar mean density, the stellar rotation rate, and the treatment of correlated noise, and were therefore not as robust as desired.¹⁷

We report here on a campaign to observe the photometric transit ingress of UT 2009 June 5, and to measure more precise RVs during the transit. We also present and analyze data that have been accumulated by the California Planet Search over the eight years since the planet's discovery. Our observations and data reduction are presented in Section 2, our analysis is described in Section 3, and the results are summarized and discussed in Section 4.

2. OBSERVATIONS

2.1. Photometry

The ingress was expected to begin between UT 23:00 June 4 and 06:00 June 5, and to last 4–5 hr. However, in June, HD 80606 is only observable from a given site for a few hours (at most) following evening twilight. To overcome this obstacle we organized a transcontinental¹⁸ campaign, with observers in Massachusetts, New Jersey, Florida, Indiana, Texas, Arizona, California, and Hawaii.

On the transit night, each observer obtained a series of images of HD 80606 and its neighbor HD 80607. In most cases, we used only a small subraster of the CCD encompassing both stars, and defocused the telescope, both of which allow an increase in the fraction of time spent collecting photons as opposed to reading out the CCD. Defocusing also has the salutary effects of averaging over pixel-to-pixel sensitivity variations, and reducing the impact of natural seeing variations on the shape of the stellar images.

Each observer also gathered images on at least one other night when the transit was not occurring to establish the baseline flux ratio between HD 80606 and HD 80607 with the same equipment, bandpass, and range of air mass as on the transit night. Details about each site are given below. (Observations were also attempted from Brookline, MA; Princeton, NJ; Lick Observatory, CA; and Winer Observatory, AZ; but no useful data were obtained at those sites due to poor weather.) In what follows, the dates are UT dates, i.e., “June 5” refers to the transit night of June 4–5 in U.S. time zones.

George R. Wallace Jr. Astrophysical Observatory, Westford, MA. Thick clouds on the transit night prevented any useful data from being obtained. However, out-of-transit data in the Cousins *R* band were obtained on June 3 using a 0.41 m telescope equipped with a POETS camera (Souza et al. 2006), and a 0.36 m telescope equipped with an SBIG STL-1001E CCD camera.

Rosemary Hill Observatory, Bronson, FL. We observed in the Sloan *i* band using the 0.76 m Tinsley telescope and SBIG ST-402ME CCD camera. Conditions were partly cloudy on the transit night, leading to several interruptions in the time series. Control data were also obtained on June 11.

De Kalb Observatory, Auburn, IN. We used a 0.41 m *f*/8.5 Ritchey–Chrétien telescope with an SBIG ST10–XME CCD camera. Data were obtained in the Cousins *R* band on May 30 and on the transit night. Conditions were clear on both nights.

McDonald Observatory, Fort Davis, TX. Two telescopes were used: the McDonald 0.8 m telescope and its Loral 2048² prime focus CCD camera with an *R_C* filter, and the MONET-North¹⁹ 1.2 m telescope with an Alta Apogee E47 CCD camera and SDSS *r* filter, controlled remotely from Göttingen, Germany. Conditions were partly cloudy on the transit night, shortening the interval of observations and causing several interruptions. Control data were obtained with the McDonald 0.8 m telescope on June 11, and with the MONET-North 1.2 m telescope on May 31 and June 4.

Fred L. Whipple Observatory, Mt. Hopkins, AZ. We used the 48 in (1.2 m) telescope and Keplercam, a 4096² Fairchild CCD camera. Cloud cover prevented observations on the transit night, but out-of-transit data were obtained on June 6 in the Sloan *riz* bands. Out-of-transit data in the *i* band were also obtained on 2009 February 13 and 14.

Mount Laguna Observatory, San Diego, CA. We observed in the Sloan *r* band with the 1.0 m telescope and 2048² CCD camera. Conditions were humid and cloudy. The target star was observable through a thin strip of clear sky for several hours after evening twilight. Out-of-transit data were obtained on June 8.

Mauna Kea Observatory, HI. We used the University of Hawaii 2.2 m telescope and the Orthogonal Parallel Transfer Imaging Camera (OPTIC; Tonry et al. 1997). Instead of defocusing, we used the charge-shifting capability of the OPTIC to spread the starlight into squares 40 pixels (5'4) on a side (Howell et al. 2003). We observed with a custom “narrow *z*” filter defining a bandpass centered at 850 nm with a full width at half-maximum of 40 nm. Out-of-transit data were obtained on June 4.

Reduction of the CCD images from each observatory involved standard procedures for bias subtraction, flat-field division, and aperture photometry. The flux of HD 80606 was divided by that of HD 80607, and the results were averaged into 10 minute bins. This degree of binning was acceptable because it sampled the ingress duration with ≈ 15 points. We estimated the uncertainty in each binned point as the standard deviation of the mean of all the individual data points contributing to the bin (ranging in number from 8 to 63 depending on the telescope). We further imposed a minimum uncertainty of 0.001 per 10 minute binned point to avoid overweighting any particular point and out of general caution about time-correlated noise that often afflicts photometric data (Pont et al. 2006). Figure 1 shows the time series of the flux ratio based on the data from the transit night of June 5, as well as the out-of-transit flux ratio derived with the same telescope.

Determining the out-of-transit flux ratio and its uncertainty was an important task. Since it was not possible to gather out-of-transit data on June 5, we needed to compare data from the same telescope that were taken on different nights. Systematic errors are expected from night-to-night differences in atmospheric conditions and detector calibrations. We believe this uncertainty to be approximately 0.002 in the flux ratio, based on the following two tests.

First, in two instances the out-of-transit flux ratio was measured on more than one night, with differences in the results

¹⁷ Gillon (2009) has submitted for publication a similar analysis of the same data, with similar results.

¹⁸ We use this term with apologies to Hawaii, which is not even on the same tectonic plate as the other sites.

¹⁹ MONET stands for MOnitoring NEtwork of Telescopes; see Hessman (2001).

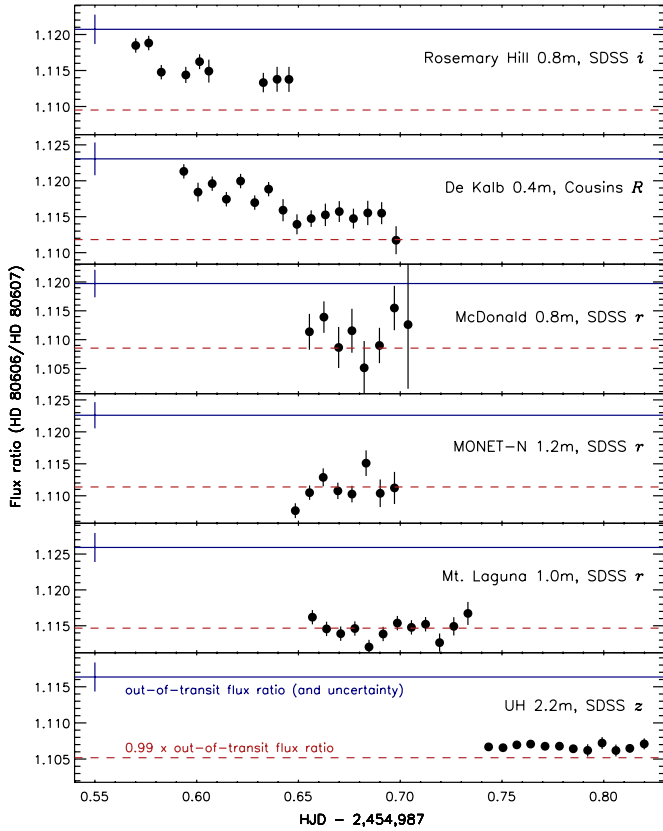


Figure 1. Flux ratio between HD 80606 and HD 80607, as measured on the transit night UT 2009 June 5. The solid blue line is the out-of-transit flux ratio as determined on a different night. The uncertainty in the out-of-transit flux ratio is indicated with an error bar on the left-hand side. The dashed red line shows the 1% drop that was expected at midtransit.

(A color version of this figure is available in the online journal.)

of 0.0004 and 0.0017 from the MONET-North and FLWO telescopes, respectively. In the latter case, the data were separated in time by 112 days, raising the possibility that longer term instabilities in the instrument or the intrinsic variability of the stars contribute to the difference, and that the night-to-night repeatability is even better than 0.0017.

A second comparison can be made by including data from *different* telescopes that employed the same nominal bandpass. This should give an upper bound (worst-case) estimate for the systematic error in the measurement from a *single* telescope on different nights. Using the data in Table 1, we asked for each bandpass: what value of σ_{sys} must be chosen in order for

$$\chi^2 = \sum_{i=1}^N \frac{(f_{\text{oot},i} - \bar{f}_{\text{oot},i})^2}{\sigma_i^2 + \sigma_{\text{sys}}^2} = N - 4, \quad (1)$$

where $f_{\text{oot},i}$ is the i th measurement of the out-of-transit flux ratio, σ_i is the statistical uncertainty in that measurement, and $\bar{f}_{\text{oot},i}$ is the unweighted mean of all the out-of-transit flux ratio measurements made in the same nominal bandpass as f_i . There are $N = 15$ data points, and $N - 4$ is used in Equation (1) because there are four independent bandpasses for which means are calculated.²⁰ In this sense, we fitted a model to the out-of-transit flux-ratio data with four free parameters. The quantities $(f_{\text{oot},i} - \bar{f}_{\text{oot},i})$ are plotted in Figure 2. The result is $\sigma_{\text{sys}} = 0.0018$.

²⁰ For this exercise, we considered the “narrow z ” band of the UH 2.2 m observations to be equivalent to the Sloan z band.

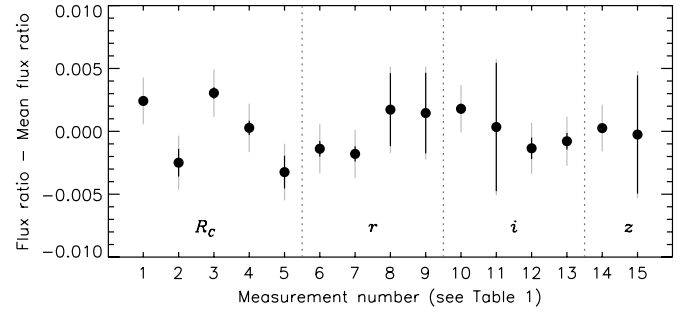


Figure 2. Deviations between the measured out-of-transit flux ratio and the mean value of the out-of-transit flux ratio across all data sets obtained with the same nominal bandpass. The data are given in Table 1. The black error bars represent statistical errors. The gray error bars have an additional systematic error of 0.0018 added in quadrature with the statistical error. The value of 0.0018 was chosen because it gives a reduced χ^2 of unity (see Equation (1)).

In our subsequent analysis, we assumed the error in the out-of-transit flux ratio to follow a Gaussian distribution with a standard deviation given by the quadrature sum of 0.0020 and statistical error given in Table 1. Given the preceding results, we believe this to be a reasonable and even a conservative estimate of the systematic error. Though it may seem too small to those readers with experience in synoptic photometry, it must be remembered that this is an unusually favorable case: the universe was kind enough to provide two stars of nearly equal brightness and color separated by only $20''$. It is also worth repeating that for our analysis we did not need to place data from *different* telescopes on the same flux scale; we needed only to align data from the *same* telescope obtained on different nights.

We pay attention to a few key aspects of the time series in Figure 1: (1) all the observers measured the flux ratio between HD 80606 and HD 80607 to be smaller on the transit night than it was on out-of-transit nights. We conclude that the transit was detected. (2) The data from Rosemary Hill and De Kalb show a decline in the relative brightness of HD 80606 over several hours. We interpret the decline as the transit ingress. (3) The data from McDonald, Mt. Laguna, and Mauna Kea show little variability over the interval of their observations, suggesting that the “bottom” (complete phase) of the transit had been reached.

2.2. Radial Velocities

We measured the relative RV of HD 80606 using the Keck I 10 m telescope on Mauna Kea, Hawaii. We used the High Resolution Echelle Spectrometer (HIRES; Vogt et al. 1994) in the standard setup of the California Planet Search program (Howard et al. 2009), as summarized here. We employed the red cross-disperser and used the iodine gas absorption cell to calibrate the instrumental response and the wavelength scale. The slit width was $0''.86$ and the exposure time ranged from 240 s to 500 s, giving a resolution of 65,000 and a typical signal-to-noise ratio of 210 pixel^{-1} . Radial velocities were measured with respect to an iodine-free spectrum, using the algorithm of Butler et al. (1996) as improved over the years.

The 73 measurements span 8 yr from 2001 to the present. Table 2 gives all of the RV data. There are 39 data points obtained prior to the upgrade of the HIRES CCDs in 2004 August, and 34 data points obtained after the upgrade. Results from the pre-upgrade data, and some of the post-upgrade data, were published by Butler et al. (2006). For our analysis, we re-reduced the post-upgrade spectra using later versions of the analysis code and spectral template. Due to known difficulties in comparing data

Table 1
Out-of-transit Flux Ratio between HD 80606 and HD 80607

Measurement Number	Observatory/Telescope	Date	Bandpass	Flux Ratio
1	University of London 0.35 m	2009 Feb 14	R_C	1.12796 ± 0.00023
2	De Kalb 0.41 m	2009 May 30	R_C	1.12305 ± 0.00110
3	Wallace 0.41 m	2009 Jun 3	R_C	1.12859 ± 0.00046
4	Wallace 0.36 m	2009 Jun 3	R_C	1.12582 ± 0.00057
5	McDonald 0.8 m	2009 Jun 11	R_C	1.12230 ± 0.00130
6	MONET-North 1.2 m	2009 May 31	r	1.12281 ± 0.00062
7	MONET-North 1.2 m	2009 Jun 4	r	1.12240 ± 0.00060
8	Mt. Laguna 1 m	2009 Jun 8	r	1.12592 ± 0.00290
9	Whipple 1.2 m	2009 Jun 6	r	1.12565 ± 0.00320
10	Rosemary Hill 0.76 m	2009 Jun 11	i	1.12072 ± 0.00041
11	Whipple 1.2 m	2009 Jun 6	i	1.11927 ± 0.00510
12	Whipple 1.2 m	2009 Feb 13	i	1.11758 ± 0.00085
13	Whipple 1.2 m	2009 Feb 14	i	1.11814 ± 0.00066
14	Mauna Kea UH 2.2 m	2009 Jun 4	830–870 nm	1.11635 ± 0.00021
15	Whipple 1.2 m	2009 Jun 6	z	1.11584 ± 0.00047

Notes. Based on data from our campaign, except for the data from the University of London Observatory which was kindly provided by Fossey et al. (2009). The quoted uncertainties represent only the “statistical error,” defined as the standard error of the mean of the flux ratios derived from all the images.

with the different detectors, we allowed for a constant velocity offset between the pre-upgrade and post-upgrade data sets in our subsequent analysis.

The post-upgrade data include nightly data from the week of the June 5 transit, which in turn include a series of eight observations taken at 30 minute intervals on the transit night. Figure 3 shows the RV data as a function of time, and Figure 4 shows the RV data as a function of orbital phase. Figure 5 is a close-up around the transit phase. Shown in all of these figures is the best-fitting model, described in Section 3.

3. ANALYSIS

We fitted a model to the photometric and RV data based on the premise of a single planet in a Keplerian orbit around a star with a quadratic limb-darkening law and uniform rotation of its photosphere. The model flux was computed using the equations of Mandel & Agol (2002). The model RV was given by $v_O(t) + \Delta v_R(t)$, where v_O is the line-of-sight component of the Keplerian orbital velocity, and Δv_R is the anomalous velocity due to the RM effect.

To compute Δv_R as a function of the orbital phase, we used the “RM calibration” procedure of Winn et al. (2005): we simulated spectra exhibiting the RM effect at various orbital phases, and then measured the apparent RV of the simulated spectra using the same algorithm used on the actual data. We found the results to be consistent with the simple formula $\Delta v_R = -(\Delta f)v_p$ (Ohta et al. 2005; Giménez 2006), where Δf is the instantaneous decline in relative flux, and v_p is the RV of the hidden portion of the photosphere.²¹

The model parameters can be divided into three groups. First are the parameters of the spectroscopic orbit: the period P , a particular midtransit time T_t , the RV semi-amplitude K , the eccentricity e , the argument of pericenter ω , and two velocity offsets γ_1 and γ_2 (for the pre-upgrade and post-upgrade data). Next are the photometric parameters: the planet-to-star radius

ratio R_p/R_* , the orbital inclination i , the scaled stellar radius R_*/a (where a is the semi-major axis), and the out-of-transit flux ratio $f_{\text{oot},i}$ specific to the data from each telescope. Finally, there are the parameters relevant to the RM effect: the projected stellar rotation rate $v \sin i_*$ and the angle λ between the sky projections of the orbital axis and the stellar rotation axis (for illustrations of the geometry, see Ohta et al. 2005, Gaudi & Winn 2007, or Fabrycky & Winn 2009). The limb-darkening (LD) coefficients were taken from the tables of Claret (2000, 2004), as appropriate for the bandpass of each data set.²²

We fitted all the Keck/HIRES RV data and all the new photometric data except the data from McDonald Observatory, which were the noisiest data and gave redundant time coverage. To complete the phase coverage of the transit, we also fitted the egress data of Fossey et al. (2009) obtained with the Celestron 0.35 m telescope, which were the most precise and exhibited the smallest degree of correlated noise.

The fitting statistic was a combination of the usual chi-squared statistic and terms representing Gaussian a priori constraints. Schematically,

$$\chi^2 = \chi_f^2 + \chi_v^2 + \chi_{\text{oot}}^2 + \chi_{\text{occ}}^2, \quad (2)$$

with the various terms defined as

$$\chi_f^2 = \sum_{i=1}^{N_f} \left[\frac{f_i(\text{obs}) - f_i(\text{calc})}{\sigma_{f,i}} \right]^2, \quad (3)$$

$$\chi_v^2 = \sum_{i=1}^{N_v} \left[\frac{v_i(\text{obs}) - v_i(\text{calc})}{\sigma_{v,i}} \right]^2, \quad (4)$$

$$\chi_{\text{oot}}^2 = \sum_{i=1}^4 \left[\frac{f_{\text{oot},i} - \bar{f}_{\text{oot},i}}{0.0020} \right]^2, \quad (5)$$

²¹ We also found this to be true for the cases of HAT-P-1 (Johnson et al. 2008) and TrES-2 (Winn et al. 2008a), although for other cases a higher order polynomial relation was needed. It is worth noting that the three systems for which the linear relation is adequate are the slowest rotators. This is consistent with the work by T. Hirano et al. (2009, in preparation) that aims at an analytic understanding of the RM calibration procedure.

²² For the R_C band, we used $u_1 = 0.3915$ and $u_2 = 0.2976$; for the r band, $u_1 = 0.4205$ and $u_2 = 0.2911$; for the i band, $u_1 = 0.3160$ and $u_2 = 0.3111$; and for the “narrow z ” band, $u_1 = 0.2424$ and $u_2 = 0.3188$. We did not allow the LD coefficients to be free parameters because the photometric data are not precise enough to give meaningful constraints on them (and conversely, even large errors in the theoretical LD coefficients have little effect on our results).

Table 2
Relative Radial Velocity Measurements of HD 80606

HJD	RV (m s ⁻¹)	Error (m s ⁻¹)
2452007.89717	-144.75	2.06
2452219.16084	-111.52	1.68
2452236.05808	-163.28	1.85
2452243.16763	-182.50	1.72
2452307.87799	505.19	1.82
2452333.00899	-114.90	1.97
2452334.01381	-126.84	1.78
2452334.90457	-127.12	1.59
2452363.02667	-193.85	1.91
2452446.75474	-121.75	1.63
2452573.12626	-170.54	1.83
2452574.15413	-170.69	2.10
2452603.13145	-237.61	1.91
2452652.07324	-27.86	1.80
2452652.99160	-31.09	1.67
2452654.04838	-47.65	1.89
2452680.96832	-163.44	1.43
2452711.77421	-232.28	2.05
2452712.83539	-237.55	1.76
2452804.81344	-181.39	2.00
2452805.81998	-180.13	2.12
2452989.05542	-60.43	1.71
2453044.89610	-234.22	1.60
2453077.07929	-330.76	2.11
2453153.73469	-233.14	1.70
2453179.74129	-294.54	1.80
2453189.74093	-338.05	1.85
2453190.73876	-354.28	1.84
2453195.73688	-408.34	1.55
2453196.74363	-423.32	1.62
2453196.75039	-421.51	1.77
2453196.75701	-420.03	1.84
2453197.73139	-444.83	2.54
2453197.73809	-427.39	1.63
2453197.74463	-429.67	1.67
2453197.75126	-436.21	1.60
2453198.73328	-232.36	3.02
2453199.73285	412.11	2.61
2453199.73960	422.80	1.76
2453398.85308	-279.18	1.06
2453425.92273	98.61	1.36
2453426.77899	65.74	1.24
2453427.02322	57.99	1.17
2453427.92202	39.16	1.19
2453428.78092	22.40	1.48
2453428.78724	21.85	1.72
2454461.95594	-148.74	2.09
2454461.96114	-153.79	1.54
2454492.97860	-228.73	1.20
2454544.94958	-8.21	0.81
2454544.95553	-6.49	0.84
2454544.96119	-4.40	0.86
2454545.95602	-16.31	1.32
2454545.96140	-22.42	1.44
2454545.96684	-20.91	1.28
2454546.84875	-27.09	0.80
2454546.85412	-27.53	0.77
2454546.85975	-28.14	0.82
2454963.87159	-299.78	1.30
2454983.75577	240.93	0.99
2454984.78842	158.39	0.97
2454985.79701	104.64	0.92
2454986.80004	72.89	0.88
2454987.74080	40.91	1.00
2454987.75055	39.72	0.92
2454987.78009	38.64	1.00

Table 2
(Continued)

HJD	RV (m s ⁻¹)	Error (m s ⁻¹)
2454987.79998	37.50	0.88
2454987.81073	36.26	1.01
2454987.82554	37.75	1.08
2454987.84052	35.98	1.09
2454987.84704	35.06	1.07
2454988.81104	25.85	0.92
2454988.81684	24.89	1.00

Notes. The RV was measured relative to an arbitrary template spectrum; only the differences are significant. The uncertainty given in Column 3 is the internal error only and does not account for any possible “stellar jitter.”

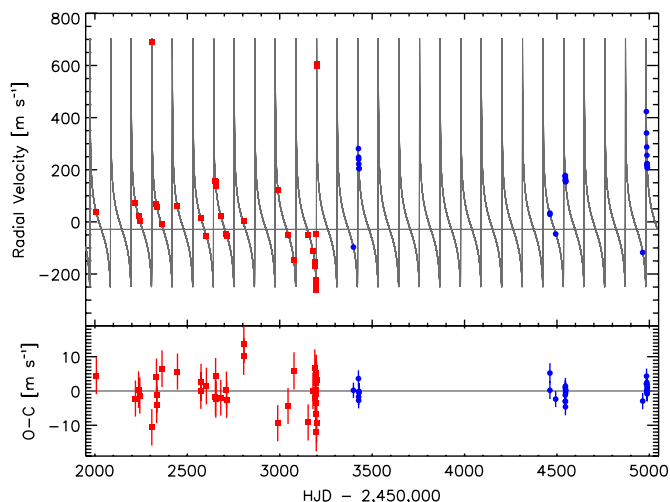


Figure 3. Radial-velocity variation of HD 80606, as a function of time. Red squares are the data obtained prior to the upgrade of the HIRES CCDs. Blue dots are the post-upgrade data. The gray line is the best-fitting model. The data were transformed into the center-of-mass frame of the star-planet system by subtracting a constant velocity offset, and the error bars represent the quadrature sum of the measurement errors quoted in Table 2 and a term representing possible systematic errors (“stellar jitter”). For the pre-upgrade and post-upgrade data, the constant velocity offsets are 184.55 and 182.45 m s⁻¹, and the systematic error terms are 5 and 2 m s⁻¹, respectively.

(A color version of this figure is available in the online journal.)

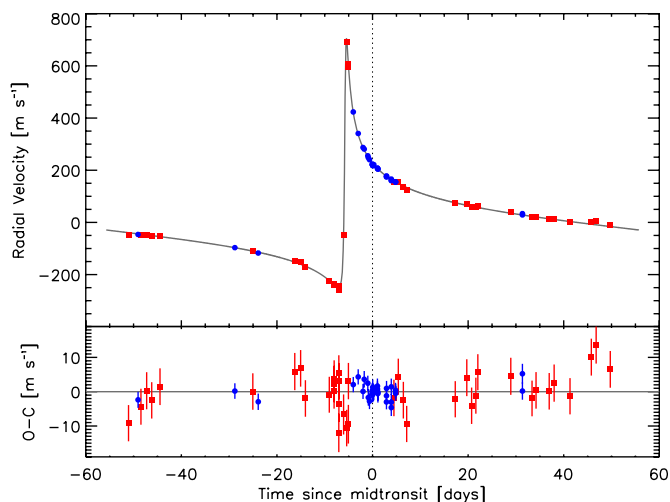


Figure 4. Radial-velocity variation of HD 80606, as a function of orbital phase. The same plotting conventions apply as in Figure 3.

(A color version of this figure is available in the online journal.)

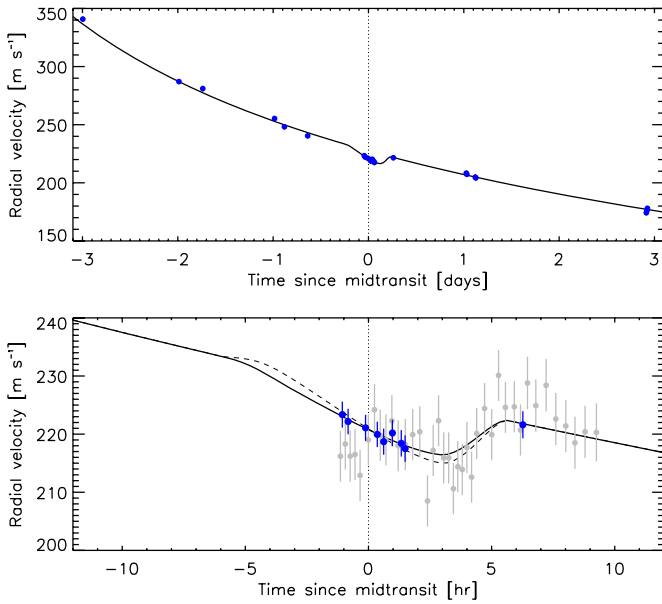


Figure 5. Radial-velocity variation of HD 80606, as a function of orbital phase, for the week of the transit (top panel) and the day of the transit (bottom panel). The in-transit RVs are all from 2009 June 5. Of the out-of-transit RVs, five are from the week of 2009 June 1–6, and the others are from different orbits. Blue dots are the post-upgrade Keck/HIRES data, after subtracting offsets and enlarging the error bars as in Figures 4 and 3. Gray dots are the SOPHIE data of Moutou et al. (2009), which were not used to derive the best-fitting models plotted here. The solid line is the best-fitting model with no prior constraint on $v \sin i_*$. The dashed line is the best-fitting model with a prior constraint on $v \sin i_*$ as explained in Section 3.

(A color version of this figure is available in the online journal.)

$$\chi_{\text{occ}}^2 = \left[\frac{T_o(\text{obs}) - T_o(\text{calc})}{\sigma_{T_o}} \right]^2 + \left[\frac{\tau_o(\text{obs}) - \tau_o(\text{calc})}{\sigma_{\tau_o}} \right]^2, \quad (6)$$

in which $f_i(\text{obs})$ is a measurement of the relative flux of HD 80606, $\sigma_{f,i}$ is the uncertainty, and $f_i(\text{calc})$ is the relative flux that is calculated for that time for a given set of model parameters. Likewise $v_i(\text{obs})$ and $\sigma_{v,i}$ are the RV measurements and uncertainties, and $v_i(\text{calc})$ is the calculated RV. The third term enforces the constraints on the out-of-transit flux ratios for each bandpass. The fourth term enforces constraints based on the measured time and duration of the occultation; we adopt the values $T_o = 2,454,424.736 \pm 0.004$ (HJD) and $\tau_o = 1.80 \pm 0.25$ hr from Laughlin et al. (2009). In contrast to previous analyses (Pont et al. 2009), we did not impose prior constraints based on theoretical stellar-evolutionary models, or on the stellar rotation rate. (In Section 4.1, we discuss how the results change if such constraints are imposed.)

For the RV uncertainties $\sigma_{v,i}$, we used the quadrature sum of the estimated measurement errors quoted in Table 2, and a term $\sigma_{v,\text{sys}}$ representing possible systematic errors. The latter term is often called “stellar jitter” and may represent Doppler shifts due to additional planets, non-Keplerian Doppler shifts due to stellar oscillations or stellar activity, as well as any errors in the instrument calibration or spectral deconvolution code. We used $\sigma_{v,\text{sys}} = 5 \text{ m s}^{-1}$ for the pre-upgrade data and $\sigma_{v,\text{sys}} = 2 \text{ m s}^{-1}$ for the post-upgrade data, based on the scatter in the observed RVs for other planet-search program stars with similar spectral types that do not have any detected planets.

With these choices, and with the flux uncertainties determined as described previously, the minimum χ^2 is 206 with 202 degrees of freedom. This indicates a good fit and suggests that

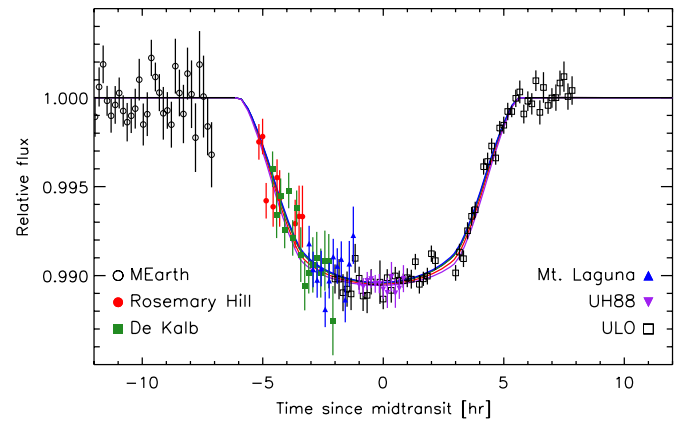


Figure 6. Photometric transit of HD 80606. The solid curves show the best-fitting model, which depends on bandpass due to limb darkening. From top to bottom the model curves are for the r , RC , i , and z bands.

(A color version of this figure is available in the online journal.)

the estimated uncertainties are reasonable. The rms scatter in the RV residuals is 5.7 m s^{-1} for the pre-upgrade data and 2.1 m s^{-1} for the post-upgrade data. The rms scatter in the photometric residuals is 0.0015, 0.0012, 0.0013, and 0.00031 for the Rosemary Hill, De Kalb, Mt. Laguna, and UH 2.2 m data, respectively.

We determined the best-fitting values of the model parameters and their uncertainties using a Markov Chain Monte Carlo algorithm (see, e.g., Tegmark et al. 2004, Gregory 2005, or Ford 2005). This algorithm creates a chain of points in parameter space by iterating a jump function, which in our case was the addition of a Gaussian random deviate to a randomly selected single parameter. If the new point has a lower χ^2 than the previous point, the jump is executed; if not, the jump is executed with probability $\exp(-\Delta\chi^2/2)$ and otherwise the current point is repeated in the chain. We set the sizes of the random deviates such that $\sim 40\%$ of jumps are executed. We created 10 chains of 10^6 links each from different starting conditions, giving for each parameter a smoothly varying a posteriori distribution and a Gelman & Rubin (1992) statistic smaller than 1.05. The phase-space density of points in the chain is an estimate of the joint a posteriori probability distribution of all the parameters, from which may be calculated the probability distribution for an individual parameter by marginalizing over all of the others.

4. RESULTS

Table 3 gives the results for the model parameters. The quoted value for each parameter is the median of the a posteriori distribution, marginalized over all other parameters. The quoted uncertainties represent 68.3% confidence limits, defined by the 15.85% and 84.15% levels of the cumulative distribution. Figure 6 shows the transit light curve and the best-fitting model. This figure also includes the MEarth observations of the 2009 February 14 transit (Pont et al. 2009), which are the most constraining of the available pre-ingress data.

4.1. Spin–Orbit Parameters

Figure 7 shows the probability distributions for the parameters describing the RM effect, $v \sin i_*$, and λ . A well-aligned system, $\lambda = 0$, can be excluded with high confidence. With 68.3% confidence, λ lies between 32° and 87° , and with 99.73% confidence, it lies between 14° and 142° . The distribution is non-Gaussian because of the correlation between λ and $v \sin i_*$.

Table 3
System Parameters of HD 80606

Parameter	Value	Uncertainty
Orbital period, P (d)	111.43740	0.00072
Midtransit time (HJD)	2, 454, 987.7842	0.0049
Transit duration (first to fourth contact) (hr)	11.64	0.25
Transit ingress or egress duration (hr)	2.60	0.18
Midoccultation time (HJD)	2, 454, 424.736	0.004
Time from occultation to transit (d)	5.8585	0.0079
Occultation duration (first to fourth contact) (hr)	1.829	0.056
Occultation ingress or egress duration (hr)	0.1725	0.0063
Velocity semiamplitude, K (m s ⁻¹)	476.1	2.2
Orbital eccentricity, e	0.93286	0.00055
Argument of pericenter, ω (deg)	300.83	0.15
Velocity offset, pre-upgrade (m s ⁻¹)	-184.58	0.93
Velocity offset, post-upgrade (m s ⁻¹)	-182.46	0.66
Heliocentric velocity (km s ⁻¹)	+3.95	0.27
Planet-to-star radius ratio, R_p/R_*	0.1033	0.0011
Orbital inclination, i (deg)	89.324	0.029
Scaled semimajor axis, a/R_*	102.4	2.9
Semimajor axis, a (AU)	0.4614	0.0047
Transit impact parameter	0.788	0.016
Occultation impact parameter	0.0870	0.0019
Projected stellar rotation rate, $v \sin i_*$ (km s ⁻¹)	1.12	-0.22,+0.44
Projected Spin–Orbit Angle, λ (deg)	53	-21,+34
Stellar Parameters:		
Mass, M_* (M_\odot)	1.05	0.032
Radius, R_* (R_\odot)	0.968	0.028
Luminosity ^b , L_* (L_\odot)	0.801	0.087
Mean density, ρ_* (g cm ⁻³)	1.63	0.15
Surface gravity, $\log g_*$ (cm s ⁻²)	4.487	0.021
Effective temperature ^b , T_{eff} (K)	5572	100
Metallicity ^b (Fe/H)	0.34	0.10
Age (Gyr)	1.6	-1.1,+1.8
Distance ^a (pc)	61.8	3.8
Planetary Parameters:		
Mass, M_p (M_{Jup})	4.20	0.11
Mass ratio, M_p/M_*	0.00382	0.00016
Radius, R_p (R_{Jup})	0.974	0.030
Mean density, ρ_p (g cm ⁻³)	5.65	0.54
Surface gravity, g_p (m s ⁻²)	110.5	8.2

Notes. Based on the joint analysis of the Keck/HIRES RV data, our new photometric data, the Celestron data of Fossey et al. (2009), and the occultation time and duration measured by Laughlin et al. (2009), except where noted.

^a Based on the apparent V magnitude of 9.06 and the luminosity implied by the stellar-evolutionary models.

^b Based on an analysis of the iodine-free Keck/HIRES spectrum using the *Spectroscopy Made Easy* (SME) spectral synthesis code; see Valenti & Piskunov (1996), Valenti & Fischer (2005).

shown in the right panel of Figure 7. No other parameter shows a significant correlation with λ .

The strong exclusion of good alignment ($\lambda = 0$) follows from the observation that the RV data gathered on June 5 were blueshifted relative to the Keplerian velocity (see Figure 5), over a time range that proved to include the midtransit time. Were the spin and orbit aligned, the anomalous RV would vanish at midtransit because the planet would then be in front of the stellar rotation axis where there is no radial component to the stellar rotation velocity. The observed blueshift at midtransit implies that the midpoint of the transit chord is on the redshifted (receding) side of the star. This can only happen if the stellar rotation axis is tilted with respect to the orbital axis.

For the projected stellar rotation rate, we find $v \sin i_* = 1.12^{+0.44}_{-0.22}$ km s⁻¹. In their previous analyses using the SOPHIE

data, Pont et al. (2009) imposed prior constraints on $v \sin i_*$ based on the observed broadening in the stellar absorption lines. This was necessary to break a degeneracy between the transit duration, $v \sin i_*$, and λ . Here we have determined $v \sin i_*$ by fitting the data exhibiting the RM effect. This is preferable whenever possible, because of systematic effects in both methods of determining $v \sin i_*$. The method based on the RM effect is subject to systematic errors in the “RM calibration” procedure (see Section 3 and Triaud et al. 2009). The method based on line broadening is subject to the systematic error because of the degeneracy between rotational broadening and other broadening mechanisms such as macroturbulence, which are of comparable or greater magnitude for slowly rotating stars such as HD 80606. These systematic effects may cause a mismatch in the results for $v \sin i_*$ obtained by the two methods,

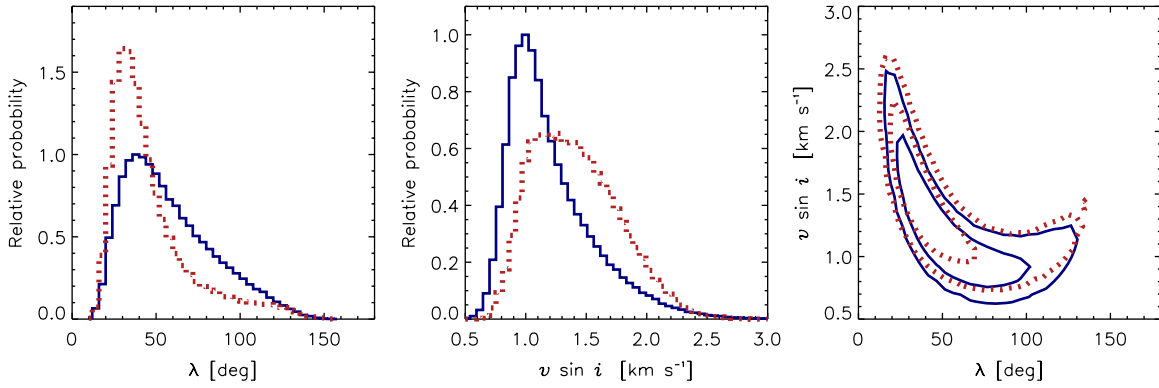


Figure 7. Probability distributions for the projected spin-orbit angle (λ) and projected stellar rotation rate ($v \sin i_*$). Blue solid curves show the results when fitting the photometry and the Keck/HIRES RVs with no prior constraint on $v \sin i_*$. Red dotted curves show the effect of applying a Gaussian prior $v \sin i_* = 1.9 \pm 0.5 \text{ km s}^{-1}$ based on analyses of the stellar absorption lines in Keck/HIRES spectra. Left: probability distribution for λ . Center: probability distribution for $v \sin i_*$. Right: joint probability distribution for $v \sin i_*$ and λ . The contours are the 68.3% and 95% confidence levels.

(A color version of this figure is available in the online journal.)

which could lead to biased results for λ if the result from the line-broadening method were applied as a constraint on the RM model.

For comparison, we review the spectroscopic determinations of $v \sin i_*$. Naef et al. (2001) found $0.9 \pm 0.6 \text{ km s}^{-1}$, based on the width of the cross-correlation function measured with the ELODIE spectrograph, after subtracting the larger “intrinsic width” due to macroturbulence and other broadening mechanisms that was estimated using the empirical calibration of Queloz et al. (1998). This result might be considered tentative, given that Queloz et al. (1998) only claim their calibration to be accurate down to $1.5\text{--}2 \text{ km s}^{-1}$. Valenti & Fischer (2005) found $v \sin i_* = 1.8 \pm 0.5 \text{ km s}^{-1}$ based on synthetic spectral fitting to the pre-upgrade Keck spectra, and a particular assumed relationship between effective temperature and macroturbulence (see their paper for details). We used the same spectral model and macroturbulence relationship to analyze one of the post-upgrade Keck spectra, finding $v \sin i_* = 2.0 \pm 0.5 \text{ km s}^{-1}$, in good agreement with Valenti & Fischer (2005) but not Naef et al. (2001).

We investigated the effect of imposing an a priori constraint on $v \sin i_*$ by adding the following term to Equation (2):

$$\chi_{\text{rot}}^2 = \left[\frac{v \sin i_* - 1.9 \text{ km s}^{-1}}{0.5 \text{ km s}^{-1}} \right]^2. \quad (7)$$

After refitting, the results for the spin-orbit parameters were $v \sin i_* = 1.37^{+0.41}_{-0.33} \text{ km s}^{-1}$ and $\lambda = 39^{+28}_{-13} \text{ deg}$. The best-fitting model is shown with a dashed line in Figure 5. The constraints on λ are tightened; the new credible interval is 25% smaller than the credible interval without the constraint. However, the improved precision does not necessarily imply improved accuracy, given the uncertainties mentioned previously regarding the RM calibration and other broadening mechanisms besides rotation. For this reason, we have emphasized the results with no external constraint on $v \sin i_*$, and provide only those results in Table 3.

The preceding results did not make use of the SOPHIE data that Moutou et al. (2009) obtained during the 2009 February transit. By leaving out the SOPHIE data, we have provided as independent a determination of λ as possible. Figure 5 shows that the SOPHIE data seem to agree with the Keck data, and with the best-fitting model constrained by the Keck data. When the SOPHIE data are fitted simultaneously with the Keck data (with

no prior constraint on $v \sin i_*$), the results for λ are sharpened to $59^{+21}_{-16} \text{ deg}$ at 68.3% confidence, and $59^{+63}_{-35} \text{ deg}$ at 99.73% confidence.

4.2. Other Parameters and Absolute Dimensions

Our orbital parameters are generally in agreement with those derived previously. One exception is the argument of pericenter, for which our result ($300.83 \pm 0.15 \text{ deg}$) is 2σ away from the result of Laughlin et al. (2009) ($300.4977 \pm 0.0045 \text{ deg}$), although the uncertainty in the latter quantity seems likely to be underestimated. Another exception is that our orbital period differs from that of Laughlin et al. (2009) by 3σ , although our period agrees with the period found by Pont et al. (2009).

The transit parameters, including the transit duration, are related directly to the stellar mean density ρ_* (Seager & Mallén-Ornelas 2003). In their previous studies, due to the poorly known transit duration, Pont et al. (2009) used theoretical expectations for ρ_* to impose constraints on their light-curve solutions. Since we have measured the transit duration, we can determine ρ_* directly from the data, finding $\rho_* = 1.63 \pm 0.15 \text{ g cm}^{-3}$.²³ This is 10%–30% larger than the Sun’s mean density of 1.41 g cm^{-3} , as expected for a metal-rich star with the observed G5 spectral type (Naef et al. 2001).

We used this new empirical determination of ρ_* in conjunction with stellar-evolutionary models to refine the estimates of the stellar mass M_* and radius R_* , which in turn lead to refined planetary parameters (see, e.g., Sozzetti et al. 2007; Holman et al. 2007). The models were based on the Yonsei–Yale series (Yi et al. 2001; Demarque et al. 2004), and were applied as described by Torres et al. (2008; with minor amendments by Carter et al. 2009). Figure 8 shows the theoretical isochrones, along with some of the observational constraints. The constraints were $\rho_* = 1.63 \pm 0.15 \text{ g cm}^{-3}$, along with $T_{\text{eff}} = 5572 \pm 100 \text{ K}$ and $[\text{Fe}/\text{H}] = +0.34 \pm 0.10$. The temperature and metallicity estimates are based on the spectroscopic analysis of Valenti & Fischer (2005), but with enlarged error bars, as per Torres et al. (2008). The results are given in Table 3.

We did not apply any constraint to the models based on the spectroscopically determined surface gravity ($\log g_*$), out of

²³ Although Seager & Mallén-Ornelas (2003) considered only circular orbits, their results are easily generalized. Needless to say, we cannot assume a circular orbit in this case and our quoted uncertainty in ρ_* incorporates the uncertainties in e and ω .

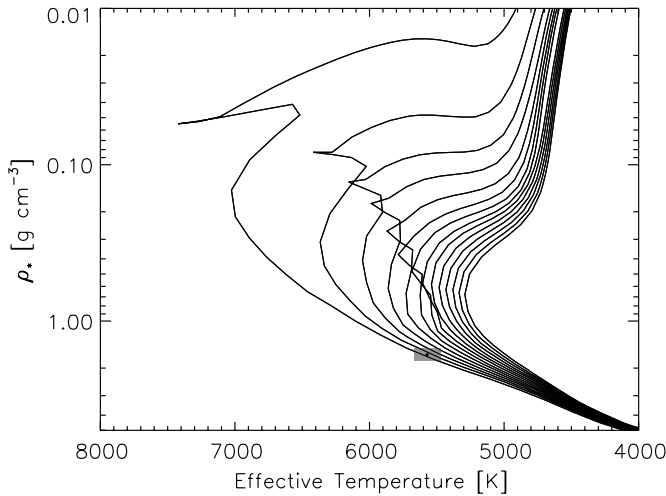


Figure 8. Stellar-evolutionary model isochrones in the space of effective temperature vs. stellar mean density from the Yonsei–Yale series by Yi et al. (2001). The point and shaded box represent the observationally determined values and 68.3% confidence intervals. Isochrones are shown for ages of 1–14 Gyr (from left to right) in steps of 1 Gyr for a fixed stellar metallicity of $[\text{Fe}/\text{H}] = 0.344$.

concern over systematic errors in that parameter (Winn et al. 2008b). Instead we performed the reverse operation: given our results for M_* and R_* we computed the implied value of $\log g_*$, finding $\log g_* = 4.487 \pm 0.021$. Reassuringly this is in agreement with, and is more precise than, the spectroscopically determined values of 4.50 ± 0.20 (Naef et al. 2001) and 4.44 ± 0.08 (Valenti & Fischer 2005).

The RVs given in Table 2 were measured with respect to an arbitrary template spectrum, and therefore they do not represent the true heliocentric RV of HD 80606, which is known much less precisely. For reference, we measured the heliocentric RV to be $\gamma = +3.95 \pm 0.27 \text{ km s}^{-1}$, using the telluric “A” and “B” absorption bands of molecular oxygen to place the Keck/HIRES spectra on the RV scale of Nidever et al. (2002). This result is in agreement with the previously reported value of $\gamma = +3.767 \text{ km s}^{-1}$ (Naef et al. 2001).

5. SUMMARY AND DISCUSSION

The poorly constrained transit duration was the main limiting factor in previous determinations of the system parameters of HD 80606b. The duration is now known to within 2.2% from a combination of the transit ingress detected in our transcontinental campaign, the photometric egress detected during the previous transit, and the orbital period that is known very precisely from the RV data. In addition, our new and more precise RV data show definitively that at midtransit the starlight is anomalously blueshifted. This is interpreted as the partial eclipse of the redshifted half of the rotating photosphere. For this to happen at midtransit, the orbital axis of the planet and the rotation axis of the star must be misaligned.

Despite these achievements, the RV signal during the later phase of the transit is known less precisely, and the RV signal during the early phase of the transit remains unmeasured. This incompleteness leads to relatively coarse bounds on the projected spin–orbit angle λ in comparison with many other systems.

As described in Section 1, the Kozai migration scenario of Wu & Murray (2003) carried an implicit prediction that the stellar spin and planetary orbit are likely to be misaligned.

In this sense, the finding of a nonzero λ corroborates the Kozai migration hypothesis. The quantitative results for λ derived in this paper are in good agreement with the theoretical spin–orbit angle of 50° predicted by Fabrycky & Tremaine (2007) in an illustrative calculation regarding HD 80606b (see their Figure 1). This agreement should not be overinterpreted, given the uncertainties in the measurement, the issue of the sky projection, and the uncertainties in some parameters of the calculation. Nevertheless the calculation demonstrates that values of λ of order 50° emerge naturally in the Kozai scenario.

The Kozai scenario is not without shortcomings. The orbital plane of the stellar binary must be finely tuned to be nearly perpendicular to the initial planetary orbit. This would be fatal to any scenario that purported to explain the majority of exoplanetary orbits, but it may be forgivable here, since we are trying to explain only one system out of the several hundred known exoplanets. Another possible problem is that (depending on the initial condition, and the characteristics of the stellar binary) the relativistic precession may have been too strong to permit Kozai oscillations (Naef et al. 2001). In this case, the theory might be rescued by the existence of a distant planet that is responsible for the Kozai effect, rather than the stellar companion. On the other hand, assuming HD 80607 is responsible, additional planets would spoil the effect. Wu & Murray (2003) used this fact to predict upper bounds on the masses and orbital distances of any additional planets.

Another mechanism that can produce large eccentricities and large spin–orbit misalignments is planet–planet scattering, in which close encounters between planets cause sudden alterations in orbital elements (Chatterjee et al. 2008; Jurić & Tremaine 2008; Nagasawa et al. 2008). However, Ford & Rasio (2008) found that planet–planet scattering rarely produces eccentricities in excess of 0.8, unless the orbit was initially eccentric (due perhaps to the Kozai effect, but without the need for such extreme tuning) or the other planet that participated in the encounter remained bound to the system.

For these reasons, further theoretical work is warranted, as is continued RV monitoring to seek evidence for additional planets. On an empirical level, it is striking that the only three exoplanetary systems known to have a strong spin–orbit misalignment all have massive planets on eccentric orbits: the present case of HD 80606b ($4.2 M_{\text{Jup}}$, $e = 0.93$), WASP–14b ($7.3 M_{\text{Jup}}$, $e = 0.09$; Joshi et al. 2009; Johnson et al. 2009), and XO–3b ($11.8 M_{\text{Jup}}$, $e = 0.26$; Johns-Krull et al. 2008; Hébrard et al. 2008; Winn et al. 2009). There are also two cases of massive planets on eccentric orbits for which λ was found to be consistent with zero: HD 17156b ($3.2 M_{\text{Jup}}$, $e = 0.68$; Cochran et al. 2008; Barbieri et al. 2008; Narita et al. 2009) and HAT-P–2b ($8.0 M_{\text{Jup}}$, $e = 0.50$; Winn et al. 2007; Loeillet et al. 2008). Thus although less massive planets on circular orbits seem to be well aligned, as a rule, it remains possible that more than half of the massive eccentric systems are misaligned. Such systems are fruitful targets for future RM observations.

We thank Carly Chubak for measuring the heliocentric RV, Debra Fischer for help with measuring $v \sin i_*$, and Dan Fabrycky for interesting discussions about the Kozai mechanism. We thank Philip Choi, Jason Eastman, Mark Everett, Scott Gaudi, Zev Gurman, Marty Hidas, Matt Holman, and Alexander Rudy, for their willingness to join this campaign even though they were not able to participate due to weather or other factors. Mark Everett, Matt Holman, and Dave Latham also helped

to gather the out-of-transit data from FLWO. We thank Bill Cochran and Ed Turner for help recruiting participants. We also thank Steve Fossey, Jonathan Irwin, and David Charbonneau for providing their data in a timely and convenient manner. We are grateful to Greg Laughlin, whose enthusiasm and persistence (and, it is suspected, a deal with the devil) led to the discovery of the eclipses of HD 80606.

Some of the data presented herein were obtained at the W. M. Keck Observatory, which is operated as a scientific partnership among the California Institute of Technology, the University of California, and the National Aeronautics and Space Administration, and was made possible by the generous financial support of the W. M. Keck Foundation. We extend special thanks to those of Hawaiian ancestry on whose sacred mountain of Mauna Kea we are privileged to be guests. Without their generous hospitality, the Keck and UH 2.2 m observations presented herein would not have been possible. The MONET network is funded by the Alfred Krupp von Bohlen und Halbach-Stiftung. W.F.W. and S.K. acknowledge support from NASA under grant NNX08AR14G issued through the Kepler Discovery Program. K.D.C., E.B.F., F.J.R., and observations from Rosemary Hill Observatory were supported by the University of Florida. Observations at Mt. Laguna Observatory were supported by the HPWREN network, funded by the National Science Foundation Grant Numbers 0087344 and 0426879 to University of California, San Diego. J.A.J. acknowledges support from an NSF Astronomy and Astrophysics Postdoctoral Fellowship (grant No. AST-0702821). Work by J.N.W. was supported by the NASA Origins program through awards NNX09AD36G and NNX09AB33G. J.N.W. also gratefully acknowledges the support of the MIT Class of 1942 Career Development Professorship.

Facilities: Keck I (HIRES) FLWO:1.2 m (Keckercam), UH:2.2 m (OPTIC), McD:0.8 m

REFERENCES

- Barbieri, M., et al. 2008, arXiv:0812.0785
- Butler, R. P., Marcy, G. W., Williams, E., McCarthy, C., Dosanji, P., & Vogt, S. S. 1996, *PASP*, **108**, 500
- Butler, R. P., et al. 2006, *ApJ*, **646**, 505
- Carter, J. A., Winn, J. N., Gilliland, R., & Holman, M. J. 2009, *ApJ*, **696**, 241
- Chatterjee, S., Ford, E. B., Matsumura, S., & Rasio, F. A. 2008, *ApJ*, **686**, 580
- Claret, A. 2000, *A&A*, **363**, 1081
- Claret, A. 2004, *A&A*, **428**, 1001
- Cochran, W. D., Redfield, S., Endl, M., & Cochran, A. L. 2008, *ApJ*, **683**, L59
- Demarque, P., Woo, J.-H., Kim, Y.-C., & Yi, S. K. 2004, *ApJS*, **155**, 667
- Fabrycky, D., & Tremaine, S. 2007, *ApJ*, **669**, 1298
- Fabrycky, D. C., & Winn, J. N. 2009, *ApJ*, **696**, 1230
- Ford, E. B. 2005, *AJ*, **129**, 1706
- Ford, E. B., & Rasio, F. A. 2008, *ApJ*, **686**, 621
- Fossey, S. J., Waldmann, I. P., & Kipping, D. M. 2009, *MNRAS*, **396**, L16
- Garcia-Melendo, E., & McCullough, P. R. 2009, *ApJ*, **698**, 558
- Gaudi, B. S., & Winn, J. N. 2007, *ApJ*, **655**, 550
- Gelman, A., & Rubin, D. B. 1992, *Stat. Sci.*, **7**, 457
- Gillon, M. 2009, arXiv:0906.4904
- Giménez, A. 2006, *ApJ*, **650**, 408
- Gregory, P. C. 2005, *ApJ*, **631**, 1198
- Hébrard, G., et al. 2008, *A&A*, **488**, 763
- Hessman, F. V. 2001, in ASP Conf. Ser. 246, Small Telescope Astronomy on Global Scales, IAU Colloq. 183, ed. B. Paczynski, W.-P. Chen, & C. Lemme (San Francisco, CA: ASP), **13**
- Holman, M. J., et al. 2007, *ApJ*, **664**, 1185
- Howard, A. W., et al. 2009, *ApJ*, **696**, 75
- Howell, S. B., Everett, M. E., Tonry, J. L., Pickles, A., & Dain, C. 2003, *PASP*, **115**, 1340
- Johns-Krull, C. M., et al. 2008, *ApJ*, **677**, 657
- Johnson, J. A., et al. 2008, *ApJ*, **686**, 649
- Johnson, J. A., et al. 2009, *PASP*, in press
- Joshi, Y. C., et al. 2009, *MNRAS*, **392**, 1532
- Jurić, M., & Tremaine, S. 2008, *ApJ*, **686**, 603
- Kozai, Y. 1962, *AJ*, **67**, 591
- Laughlin, G., Deming, D., Langton, J., Kasen, D., Vogt, S., Butler, P., Rivera, E., & Meschiri, S. 2009, *Nature*, **457**, 562
- Lissauer, J. J. 1995, *Icarus*, **114**, 217
- Loeillet, B., et al. 2008, *A&A*, **481**, 529
- Mandel, K., & Agol, E. 2002, *ApJ*, **580**, L171
- McLaughlin, D. B. 1924, *ApJ*, **60**, 22
- Moutou, C., et al. 2009, *A&A*, **498**, L5
- Naef, D., et al. 2001, *A&A*, **375**, L27
- Nagasawa, M., Ida, S., & Bessho, T. 2008, *ApJ*, **678**, 498
- Narita, N., et al. 2009, *PASJ*, in press (arXiv:0905.4727)
- Nidever, D. L., Marcy, G. W., Butler, R. P., Fischer, D. A., & Vogt, S. S. 2002, *ApJS*, **141**, 503
- Ohta, Y., Taruya, A., & Suto, Y. 2005, *ApJ*, **622**, 1118
- Pont, F., Hébrard, G., Irwin, J. M., Bouchy, F., Moutou, C., Ehrenreich, D., Guillot, T., & Aigrain, S. 2009, *A&A*, **502**, 695
- Pont, F., Zucker, S., & Queloz, D. 2006, *MNRAS*, **373**, 231
- Queloz, D., Allain, S., Mermilliod, J.-C., Bouvier, J., & Mayor, M. 1998, *A&A*, **335**, 183
- Queloz, D., Eggenberger, A., Mayor, M., Perrier, C., Beuzit, J. L., Naef, D., Sivan, J. P., & Udry, S. 2000, *A&A*, **359**, L13
- Rossiter, R. A. 1924, *ApJ*, **60**, 15
- Seager, S., & Mallén-Ornelas, G. 2003, *ApJ*, **585**, 1038
- Souza, S. P., Babcock, B. A., Pasachoff, J. M., Gulbis, A. A. S., Elliot, J. L., Person, M. J., & Gangestad, J. W. 2006, *PASP*, **118**, 1550
- Sozzetti, A., Torres, G., Charbonneau, D., Latham, D. W., Holman, M. J., Winn, J. N., Laird, J. B., & O'Donovan, F. T. 2007, *ApJ*, **664**, 1190
- Tegmark, M., et al. 2004, *Phys. Rev. D*, **69**, 103501
- Tonry, J., Burke, B. E., & Schechter, P. L. 1997, *PASP*, **109**, 1154
- Torres, G., Winn, J. N., & Holman, M. J. 2008, *ApJ*, **677**, 1324
- Triaud, A. H. M. J., et al. 2009, *A&A*, in press (arXiv:0907.2956)
- Valenti, J. A., & Fischer, D. A. 2005, *ApJS*, **159**, 141
- Valenti, J. A., & Piskunov, N. 1996, *A&AS*, **118**, 595
- Vogt, S. S., et al. 1994, *Proc. SPIE*, **2198**, 362
- Winn, J. N., et al. 2005, *ApJ*, **631**, 1215
- Winn, J. N., et al. 2007, *ApJ*, **665**, L167
- Winn, J. N., et al. 2008a, *ApJ*, **682**, 1283
- Winn, J. N., et al. 2008b, *ApJ*, **683**, 1076
- Winn, J. N., et al. 2009, *ApJ*, **700**, 302
- Wu, Y., & Murray, N. 2003, *ApJ*, **589**, 605
- Yi, S., Demarque, P., Kim, Y.-C., Lee, Y.-W., Ree, C. H., Lejeune, T., & Barnes, S. 2001, *ApJS*, **136**, 417